

Robust 3D Texture Classifier using Score Block Operations

Mira Park

School of Design, Communication and IT, University of Newcastle, Australia

Summary

This paper presents a scheme of analyzing lung texture to solve the problem of identifying undefined patterns and distinguishing the complex background of superimposed structures in chest radiographs. The method detects and quantifies the interstitial abnormalities in a chest radiograph using the contents based image retrieval (CBIR) scheme. This technique is based on the image feature vector obtained from quasi-Gabor filters and a 3D structure classification scheme. The quasi-Gabor filters are capable of maintaining low computational cost while keeping the important information of the power spectrum of 2D-DFFT, such as band-pass frequency and direction of texture. The 3D classifier is able to capture not only local texture but also global distribution of lung texture and it overcomes the existing problems of a general block operation such as sliding block operation. Our method is a generic one in the sense that it could be applied to analyze the texture of any other images including natural scenery and various medical images such as CT or MRI images.

Key words:

Chest radiograph, texture, score block operation.

1. Introduction

The importance of recognizing patterns of diffuse pulmonary lung disease on the chest radiograph cannot be over emphasized. Many qualified radiologists could miss the abnormal patterns since the patterns deviate only slightly from the normal patterns. Computer aided diagnosis (CAD) can provide a second opinion and increase the success rate in reading and interpreting chest radiographs. The radiologist usually looks at a specific feature rather than a general feature but CAD could suggest many features to look at. The radiologist sometimes finds a new abnormal feature and can have help from CAD which is able to look at the past database to automatically check the new abnormality.

To interpret lung patterns, the radiologists often employ local properties like perceived intensity, uniformity, roughness, regularity, directionality, coarseness, smoothness and granulation [12]. For detection and characterization of these properties in radiological images, it is very important to categorize the abnormalities [2, 3, 4]. For radiology, the quantification of the image features of

normal and/or abnormal lung patterns is certainly more complicated. Indeed, the patterns in the abnormalities are ill-defined, complex, and their variations are complicated [47]. Especially as they are often superimposed with other structures such as rib cages and vessels.

A number of CAD researchers have proposed the lung texture analysis of radiographs [13, 14, 1, 8, 9, 31, 30, 10, 16, 24, 32, 33, 34]. Revesz [40] and Stark [42] investigated the feasibility of classification of the lung texture based on an optical Fourier transform power spectrum. Tully [44], Kruger [29] and Turner [45] used co-occurrence matrices to classify the regions of interest (ROIs). Jagoe and Patton [17] explored the use of features based on the magnitude and direction of the gradient in several studies [17, 18, 19]. Katsuragawa [20, 21, 22] used the root-mean-square variation and the first moment of the power spectrum as physical measures to detect and characterize interstitial abnormalities. Kido *et al* [25] computed geometric features, similar to the method later described in Katsuragawa [23] and [26, 27] Kido.

There are problems with the above mentioned methods. All these methods are designed for the special characteristics of the lung texture in chest radiographs to restrict texture analysis to regions of interest (ROIs) that do not contain normal structures such as (crossing) rib borders and (large) vessel projections. Ginneken [13, 14] proposed a method based on texture analysis on local regions in the image and the detection is not restricted to any ROIs.

The method proposed in this paper detects and quantifies the interstitial abnormalities in a chest radiograph using the contents based image retrieval (CBIR) scheme. This technique is based on the image feature vector obtained from *quasi*-Gabor filters and a 3D structure classification scheme. Our approach differs from Ginneken's method to overcome the above problems since the lung region segmentation is not needed to employ local and global properties. Our approach does not require any predefined patterns and is not limited to a chest radiograph; the method could be applied to any other natural scenery and various medical images.

2. Materials

The database used for this study includes 31 posteroanterior (PA) 14"×17" chest radiographs including 13 normal and 18 abnormal, selected in the Department of Radiology, St Vincents Hospital. In order to train classifiers to distinguish between different patterns, the radiologist has outlined the most clear areas containing dots or grape-like patterns in each abnormal image. Abnormal images contain 8 images with dots pattern, 7 images with grape-like pattern and 3 images with both dots and grape-like patterns. All images were read by an experienced radiologist. The digital images were obtained by digitizing the chest radiographs with a Kodak Lumisys Film Digitizer. The original digitized image has a pixel size of 0.175 mm, a matrix size of 2048×2487 pixels, and 12 bits gray level range.

3. Methods

3.1 System Overview

The system segments the right and left lung fields. A raster-scan convolution on input image is performed with step size at 32 when the block size is 128×128 to process the texture analysis algorithm on one block at a time. The block is transformed using 2D-DFFT to obtain a power spectrum. A 42 dimension feature vector is formed from the power spectrum through the 42 channels of a *quasi*-Gabor filter and is normalized along the frequency range 0 to 1. The system then classifies the feature vector based on contents-based image retrieval scheme. The class value of the feature vector is assigned to the whole block and a part (cell) of the block is classified using 3D classifier with score block operation. After a raster-scan convolution, the classified lung field is divided into 3 regions which are upper-, middle- and lower-lung. The final classification is executed for each region. Figure 1 shows the system overview block diagram.

3.2 Segmentation of lung fields

The right and left lung fields are automatically extracted using a knowledge based method [5, 35]. The outside region of each lung is set to a very high intensity, which is higher than the maximum intensity of the radiograph, for the background that is the non lung region.

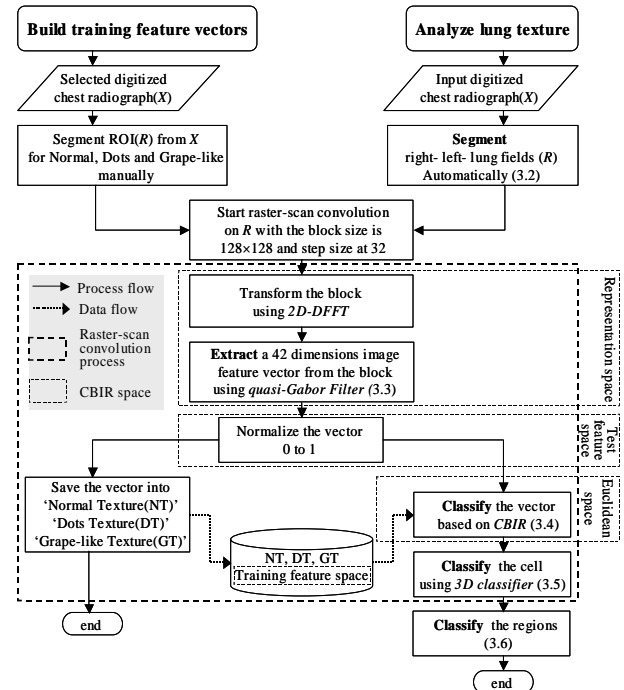


Fig. 1 System overview

3.3 Texture analysis

The texture feature vector is derived with the *quasi*-Gabor filter [36, 37]. Our *quasi*-Gabor filters consist of 42 channels. There are six frequency channels ($f = 1, 2, 4, 8, 16$ and 32), and seven orientation channels ($\theta = 0^\circ, 36^\circ, 72^\circ, 108^\circ, 144^\circ, 45^\circ$ and 135°). Each channel is either a square or a rectangle in the frequency domain, as shown in Figure 2. The value of the channel is the mean spectrum of the region, ie,

$$v_f^\theta = \frac{1}{A} \begin{pmatrix} \sum_{f+\cos\theta \cdot s \cdot \log_2(f)} & \sum_{f+\cos\theta \cdot s \cdot \log_2(f)} & \\ \sum_{x=\cos\theta \cdot s \cdot \log_2(f)} & \sum_{y=\cos\theta \cdot s \cdot \log_2(f)} & I(x, y) \end{pmatrix} \quad (1)$$

where A is the size of the block $(f \times 2^{n-7}) \times (f \times 2^{n-7})$, s is $f \times (2^{n-7})$ when the size of the image is $2^n \times 2^n$. Blocks at $0^\circ, 36^\circ, 72^\circ, 108^\circ$ and 144° are a full size square and the blocks at 45° and 135° are rectangles half the size of the square. Using the *quasi*-Gabor filters, it is much faster ($O(n \log(n))$) than using Gabor filters ($O(n^2)$) [45, 46] or other filters.

3.4 Classifying texture feature vectors

Our texture analysis system adopts the content-based image retrieval scheme. Our system consists of three

spaces which are representation space, feature space and Euclidean space. Representation space uses image processing feature extraction methods in order to represent a given image. After having characterized an image as a point in a multidimensional vector, feature space maintains the vector. There are two feature spaces which are test feature space and training feature space. Test feature space maintains a query vector. Training feature space is constructed for normal, dots and grape-like patterns. When a query feature vector is presented to Euclidean space, the k nearest neighbors of the query feature vector are retrieved from the training feature space. If there are k neighbors and $\{c_1, \dots, c_k\}$ are the classes of the k neighbors, with ω_1 for normal, ω_2 for dots and ω_3 for grape-like patterns, the classification for the query feature vector is

$$c_{vector} = modal\{c_1, \dots, c_k\} \quad (2)$$

where $modal\{\}$ is the index of the maximum value of the set.

3.5 Classifying the cell using 3D classifier

Image segmentation for both natural images and medical images by texture processing usually involves processing an image in sections called blocks, rather than processing the entire image at once. The blocks have the same size across the image. Every pixel within each large block was assigned the same texture values. There is no overlap between the blocks. This is called distinct block operation. This leads to a significant loss of resolution that is especially unacceptable in medical imaging [28]. An alternate method was used where the texture values were assigned to a pixel by using a window centered about that pixel [41]. This is called sliding neighborhood operation. There are three considerable problems of this operation.

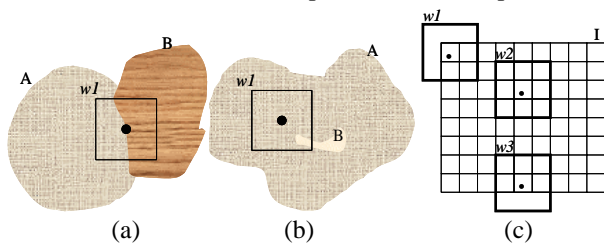


Fig 2. Possible problematic examples

The first problem occurs near the border of different textures. The pixel in the center of window $w1$ in Figure 2(a) is assigned a value calculated from both textures A and B, which could be neither A nor B.

The second problem occurs at the neighbor of high strong texture. Strong texture means its texture value is highly distinguishable, especially with high intensity, so the pixel in the center of window $w1$ in Figure 2(b) can be classified

as B when the texture of B is more stronger than texture A. This usually happens when Fourier spectra is used for texture analysis and if the texture has a high spectrum.

The third problem occurs at the boundary of an image or a segmented image. When an image operation is performed over the boundary of an image some of the pixels in a neighborhood may be missing, especially when the center pixel is on the corner of the image (see $w1$ and $w3$ in Figure 2.c). To process these neighborhoods, sliding neighborhood operations pad the borders of the image, usually with 0's (15Gonzalez 1993). This can lead to an imprecise result for those areas.

In order to overcome the bottleneck of classification discussed above, we propose a 3D classifier [39] with score block operation [38] without changing the underlying feature extraction mechanism.

Score block operation is like distinct block operation since once the block is classified as a *class c*, every pixel within each block was assigned the same *class c*. The block then slides by m pixels, where $1 \leq m \leq \beta$ when the block size is $\beta \times \beta$. β is 2^N where $N = 0, 1, 2, \dots$ and m is $\beta/2^n$ ($= 2^{N-n}$) where $n \leq N$ and $n = 0, 1, 2, \dots$, therefore the probability of the overlap areas is

$$P_{overlap} = \frac{\beta - m}{\beta} \quad (3)$$

In score block operation, $m \times m$ is the smallest unit to classify the image and it is called a *cell*. If m is 1, the block moves only one pixel and the cell classifier is performed based on a pixel. If m is β as a maximum, the block moves β pixels, so it becomes the same method with distinct block operation. The most important key point of this approach is to hold all possible classes on the overlap areas instead of overwriting with later classification. To achieve this, 3D cell classifier is presented. Each cell maintains a score stream to collect votes for a certain class regarding the texture values. Therefore, the length of score stream depends on the possible number of classes. Figure 3(a) shows 2d square image to illustrate score block operation. The image size is unknown and one cell represents $m \times m$ pixels. The block size is $m\beta \times m\beta$ pixels in this example. When the block moves by m pixel(s) (one cell in Figure 3.a), the numbers in each cell denote the frequency of overlap by the number of blocks. The cell collects votes of the class to store in the score stream. In this case the maximum frequency of overlap is β^2 . Figure 3(b) shows a score block operation example with an irregular shaped image, for example a segmented image such as a lung field in a chest radiograph. The block size is $m \times 4$ pixels, and the block moves by m pixel(s), so the maximum chance to collect votes for cells in this image is $4^2 (=16)$.

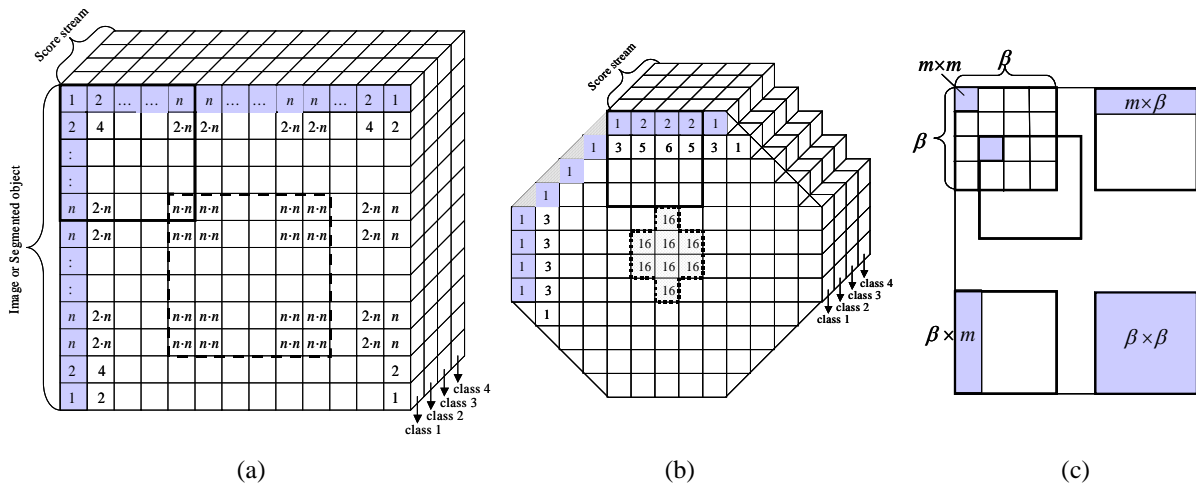


Fig 3. Referenced frequencies board with score stream.
 (a) presents a square shape of 2d image example with 4 possible classes.
 (b) presents an irregular shape of 2d image example.
 (c) presents 4 classification cases regarding the location of the block.

We do a raster-scan convolution on input image with step size at m . The 3D classifier has two phases as follows:

phase 1. collect votes for cells

- process one block at a time
- classify the texture feature vector of the block
- collect votes for a certain class for the score stream in each cell of the whole block

phase 2. classify cells

- decide a *range* to be classified
 - if** the block reaches the bottom-right corner
 $range \leftarrow index(i,j) \text{ to } index(i+\beta-1, j+\beta-1)$
 - else if** the block reaches the bottom
 $range \leftarrow index(i,j) \text{ to } index(i+m-1, j+\beta-1)$
 - else if** the block reaches the right boundary
 $range \leftarrow index(i,j) \text{ to } index(i+\beta-1, j+m-1)$
 - else**
 $range \leftarrow index(i,j) \text{ to } index(i+m-1, j+m-1)$
- classify the range to the most frequent score in the score streams of cells

Cell classification should be performed before a block moves to the next position. When processing is finished on a block, a part of the block can be classified according to its collecting votes in score stream. There are four cases to select a part of the block to classify that part. When a block reaches the right of an image, the first top row cells of the block can be classified. When a block reaches the bottom of an image, the left most column cells of the block can be classified. When a block reaches the right-bottom of an image, the whole cells in the block can be classified. For all other cases, only one left-top cell of the

block can be classified (see Figure 3.c). The classification for each cell is

$$c_{cell} = modal\{ScoreStream_{cell}\} \quad (4)$$

where $modal\{\}$ is the index of the maximum value of the set.

3.6 Classifying region

The texture analysis is processed on the segmented lung, then the classified lung field is simply segmented into three regions which are upper, middle and lower. The final classification for each region is

$$c_{region} = modal\{region\} \quad (5)$$

However, for analyzing a chest radiograph it is a bit different from other general images since even though the maximum number of classes is normal class, the system can not report the region is normal if there are any abnormalities. Therefore, to classify the regions when there are three classes $\omega_1 = \text{normal}$, $\omega_2 = \text{dots}$ and $\omega_3 = \text{grape-like}$, the classification is

$$c_{region} = \begin{cases} \omega_1 & \text{for } (modal\{region\}) \neq \{\omega_2 \text{ or } \omega_3\} \\ modal\{region, [\omega_2, \omega_3]\} & \end{cases} \quad (6)$$

where $modal\{a, [b]\}$ is the index of the maximum value of the set a and the index value must belong to set b .

4. Performance analysis and discussion

4.1 Experiment arrangement

Evaluation of diffuse interstitial disease in chest radiographs is one of the most difficult problems in diagnostic radiology. This difficulty is due to: (a) the numerous patterns and complex variations that are involved, and (b) variations among radiologists in the terms that they use to describe radiographic patterns, and which are not defined objectively [22]. The typical descriptions of the patterns are termed linear, reticular, reticulonodular, ground glass, mottled, military, or honeycomb [11]. To simplify the problem, we group the patterns into dots, grape-like and honeycomb and thus dots pattern refers to small irregular (reticular) pattern, and grape-like or honeycomb pattern refers to alveolar (air space) pattern. A mixture of patterns would be recognizable radiographically. As a general rule, it is safer for the radiologist to select the predominant pattern as the basis for differential diagnosis, so our system recognizes the most pixels of a certain pattern as the predominant pattern. The evaluation of our diffuse interstitial texture concurs radiologists' view. Radiologists describe the texture as follows:

'Probably PCP (Pneumocystic Carinii Pneumonia), more lung markings (dots and lines) in both lower lung fields, suggests an interstitial process.'

While a radiologist can outline the clearest abnormal areas in the abnormal images, it is not easy to precisely outline the actual abnormal area. Therefore, our system analyzes the texture based on the parts of the lung such as upper-right lung, middle-right lung, lower-right lung, etc.,. If our system detects *grape-like* texture in middle-right lung, the system reports the middle-right lung has *grape-like* texture. If there is more than one texture such as grape-like and dots texture, our system reports more pixel patterns. We then compare this result with a radiologist's result. If our result is the same as the radiologist's, it is a true positive. If the result is not the same as the radiologist's, it is a false positive or a false negative.

The resulting database contains 186 (31 radiographs \times 2 lungs \times 3 parts) sub-images since a chest radiograph is segmented into the right lung and left lung and each lung is divided into the upper, middle and lower lung. A radiologist usually says the lung abnormalities occur at the right-upper, the right-middle, the right-lower, the left-upper, the left-middle, and the left-lower, so our system is able to report using the terms found in radiology reports. 186 sub-images include 122 normal, 28 dots and 36 grape-like patterns. The sub-image database does not include honeycomb patterns.

The training feature vectors are extracted from one normal image, an image with dots patterns image and an image with grape-like pattern image. From the normal image ($n = 376$), from dots pattern image ($n = 189$) and from grape-like image ($n = 270$), image feature vectors are extracted. These training sets are obtained from the actual images, so there is no need to define the patterns. When the unknown patterns are detected from the testing sets, the patterns can be simply added to the training sets.

We used 2 test sets generated from four methods for the accuracy testing. Method 1 used the 42 dimensions image feature vectors and three classes including normal texture (NT), dots texture (DT) and grape-like texture (GT). Method 2 used the 42 dimensions image feature vectors and two classes including NT and the abnormal texture (AT) class. AT simply adds DT and GT, so the system only needs to detect the normal texture and abnormal texture which includes the dots texture and grape-like texture. Method 3 used the 21 dimensions image feature vectors selected from the whole vector's $f = 8, 16, 32$ and three classes including NT, DT and GT. We tested the vector at high frequencies ($f = 8, 16, 32$) because the patterns in the vector are more clear at high frequencies than at low frequencies ($f = 1, 2, 4$). Method 4 used the 21 dimensions feature vectors which is the same vector of method 3 and two classes which are NT and AT. The first set of method 1 to 4 used 3D classifier with score block operation. The second set of method 1 to 4 used the slide block operation.

Lung segmentation is beyond the scope of this paper. Interested readers can look at Brown *et al* [5] and Park *et al* [35].

4.2 Results

We tested various block sizes from 64×64 to 512×512 . We selected 128×128 pixels block since the performance was the best compared to other size blocks. Small block size is useful to process a narrow area such as around sharp edges (costophrenic angle), but the blocks smaller than 128×128 do not capture enough texture information, so the performance is low. Blocks larger than 128×128 pixels possess too much texture information, so the performance with this block size was not acceptable.

Score block operation assigns the same texture value to every pixel within each is just like a distinct block operation. This property enables us to classify the boundary of an image (or a segmented image) based on its true texture since it does not need to include dummy pixels with '0' for padding. Our block operation also overlaps between the blocks like sliding block operation since the block is sliding by m pixels. These overlap areas can control the resolution of a classified image. If m is 1, the resulting image will have a very high resolution, but there

Table 1: Result for all testing sets using method1 and method 3

Radiologist	Normal			Dots			Grape-like		
	122			28			36		
	correct identification	false dots	false grape-like	correct identification	false normal	false grape-like	correct identification	false normal	false dots
Method1	86 (70.5%)	1 (0.8%)	35 (28.7%)	7 (25%)	5 (17.8%)	16 (57.1%)	34 (94.4%)	1 (2.8%)	1 (2.8%)
Method3	84 (68.9%)	3 (2.4%)	35 (28.7%)	6 (21.4%)	6 (21.4%)	16 (57.1%)	31 (86.1%)	1 (2.8%)	4 (11.1%)

Table 1: Result for all testing sets using method2 and method 4

Radiologist	Normal		Abnormal	
	122		64	
	correct identification	false abnormal	correct identification	false normal
Method2	86 (70.5%)	36 (29.5%)	58 (90.6%)	6 (9.4%)
Method4	84 (68.9%)	38 (31.1%)	57 (89.1%)	7 (10.9%)



(a) normal image (dis01)



(b) abnormal image (dis21)

Fig 4. The example images for testing sets

are too many unnecessary overlaps. If m is β , it is just like distinct block operation with very low resolution results. We choose $m = 32$ from our experiments, which means our system allows 75% overlap.

When $k=1$ to 5, the results are not much different because a block moves one or two pixels to build the training feature vectors so the feature vectors are very close to each other. Therefore, we finally selected $k=5$, $\beta=128$, and $m=32$.

Tables 1 and 2 show the results, which were compared with the most experienced radiologist's diagnosis. For the normal pattern, method 1 and 2 are better than method 3 and 4. That means the whole 42 features vector is better to represent normal pattern than partial 21 features vector. 28.7% of normal patterns were recognized as grape-like pattern and 0.8% of normal patterns were recognized as dots patterns. These false negatives occurred around the hilar region or around the clavicles. These areas show a more complicated structure in both normal and abnormal images. The false positive rate for the normal pattern

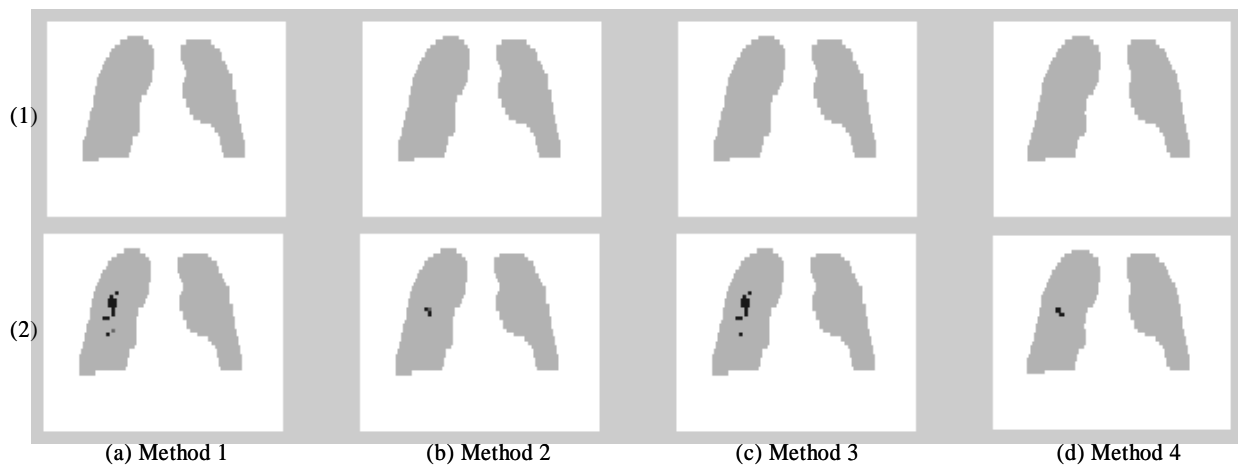


Fig 5. Result dis01: (1) use score block operation (2) use sliding block operation

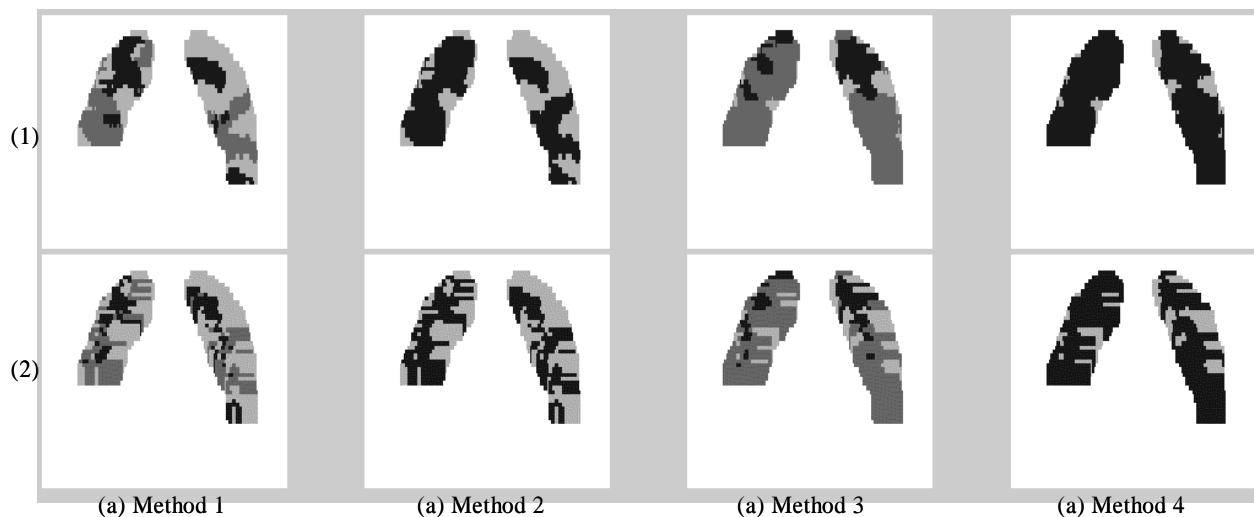


Fig 6. Result dis23: (1) use score block operation (2) use sliding block operation

regarding dots pattern is 17.8%. This high error rate is because we have very clear dots pattern training feature vectors in our vector base but the testing images including dots pattern can vary from close to the training dots pattern images to close to the normal image. Therefore, to reduce the false positive rate for normal pattern, a more precise classification scheme to construct the training sets and testing sets is needed. For the same reason, the true positive rate of dots pattern is 25% which is very low. The testing images including dots patterns, which were indicated by a radiologist, are not clearly categorized. Those images are still bound with normal images and grape-like pattern images. The best result, 94.4%, is shown when grape-like pattern was detected using method 1. This result actually is very remarkable since the training

feature vectors were built from both left- and right-lung of one image and 34 regions were detected. Only 2 regions were missed.

The first row of Figure 5 and 6 show the results from set 1, which used 3D classifier with score block operation, and the second row of the figures shows the result from set 2, which used a sliding block operation. The first column to the last column of the figures presents the result for method 1, 2, 3 and 4. Figure 5 shows the classified image of the normal lung in Figure 4(a). As the result shows, the normal image is clearly classified as normal pattern by our new classifier. Figure 6 shows the classified image of the abnormal lung in Figure 4(b), which includes grape-like and dots pattern. The most dark parts indicate grape-like pattern and the middle gray parts indicate dots pattern. The

results by method 2 and 4 only show normal and abnormal (grape-like and dots) patterns, so black areas indicate abnormal pattern and gray areas indicate normal pattern. The result with sliding block operation also detects the abnormal patterns but the area looks like a combination of several patterns. Therefore, the difference between our method and sliding block operation is the precision of classification result and the results are clearly visible. The results regarding the whole lungs are 10 true positives out of 13 normal images and 16 true positives out of 18 abnormal images among the 31 PA chest radiographs database.

5. Conclusion

We have presented *quasi*-Gabor filters to analyze the lung texture and a 3D structure classification scheme with score block operation to classify the lung texture in chest radiographs. The CBIR scheme was adopted to classify image feature vectors and to solve the problem of identifying undefined patterns and distinguishing the complex background of superimposed structures of lung fields. The *quasi*-Gabor filters are capable to maintain low computational cost while they keep the important information in the power spectrum of 2D-DFFT, such as a band-pass frequency and a direction of texture. The 3D classifier with score block operation successfully performed to capture not only local texture but also global distribution of lung texture and it overcame the existing problems of a general block operation such as sliding block operation. Our method is a generic one in the sense that it could be applied to analyze the texture of any other images including natural scenery and various medical images such as CT or MRI images.

Acknowledgments

The authors would like to thank Dr. Doust Bruce of St. Vincent Hospital, Sydney, Australia, for supplying all radiographs, annotating them and providing invaluable medical verification advice.

References

- [1] Aoyama M., Li Q., Katsuragawa S., MacMahon H. and Doi K. Automated Computerized Scheme for Distinction Between Benign and Malignant Solitary Pulmonary Nodules on Chest Images, *Medical Physics*, 29(5):701-708, 2002
- [2] Arimura H., Katsuragawa S., Li Q., Ishida T., and Doi K. Development of a computerized method for identifying the posteroanterior and lateral views of chest radiographs by use of a template matching technique, *Medical Physics*, 29(7):1556-1561, 2002
- [3] Armato G.S., Giger L.M. and MacMahon H. Computerized Detection of Abnormal Asymmetry in Digital Chest Radiographs, *Medical Physics*, 21(11):1761-1768, 1994
- [4] Baydush H.A., Catarious M.D., Lo Y.J., Abbey K.C. and Floyd E.C. Computerized Classification of Suspicious Regions in Chest Radiographs using Subregion Hotelling Observers, *Medical Physics*, 28(12):2403-2409, 2001
- [5] Brown S.M., Wilson S.L., Doust D.B., Gill W.R. and Sun S. Knowledge-Based Method for Segmentation and Analysis of Lung Boundaries in Chest X-ray Images, *Computerized Medical Imaging and Graphics*, 22:463-477, 1998
- [6] Chernov M.V. A Metric Unified Treatment of Two-Dimension FFT, 662-669, 1996
- [7] Cooley, J. W. and Tukey, J. W. An algorithm for the machine calculation of complex Fourier series, *Mathematics of Computation*, 19(90):297-301, 1965
- [8] Copley J.S., Wells U.A. Rubens B.M. Chabat F., Sheehan E.R., Musk W. and Hansell M. Functional Consequences of Pleural Disease Evaluated with Chest Radiography and CT, *Radiology*, 220(1):237-243, 2001
- [9] Cox G.S., Hoare F.J. and Jager G. Experiments in Lung Cancer Nodule Detection using Texture Analysis and Neural Network Classifiers, Third South African Workshop on Pattern Recognition, 1992
- [10] Doi K., MacMahon H., Nakamori N., Sasaki Y. and Fennessy J.J. Quantitative Computer-Aided Analysis of Lung Texture in Chest Radiographs, *RadioGraphics*, 10:257-269, 1990
- [11] Felson B. *Chest Roentgenology*, W.B. Saunders, 1973
- [12] Fenstad M.A., Lundervold A., Bock M. and Schad R.L. How Does the Signal-to-Noise Ratio Influence Texture Measures, 8th Meeting of the ISMRM, 2000
- [13] Ginneken B. *Computer-Aided Diagnosis in Chest Radiography*, Thesis University Medical Center Utrecht, 2001
- [14] Ginneken B., Katsuragawa S., Romeny B., Doi K. and Viergever M. Automatic Detection of Abnormalities in Chest Radiographs Using Local Texture Analysis, *IEEE Transactions on Medical Imaging*, 21(2):139-149, 2002
- [15] Gonzalez R.C and Woods R.E. *Digital Image Processing*, Addison-Wesley Publishing Company, 1993
- [16] Ishida T., Katsuragawa S., Nakamura K., MacMahon H. and Doi K. Computerized Analysis of Interstitial Disease in Chest Radiographs: Improvement of Geometric-Pattern Feature Analysis, *Medical Physics*, 24(6):915-, 1997
- [17] Jagoe J.R. and Patton K.A. Reading Chest Radiographs for Pneumoconiosis by Computer, *British Journal of Industrial Medicine*, 32:267-272, 1975
- [18] Jagoe J.R. and Patton K.A. Measurement of Pneumoconiosis by Computer, *IEEE Transactions on Computers*, 25:95-97, 1976
- [19] Jagoe J.R. Gradient Pattern Coding - An Application to the Measurement of Pneumoconiosis in Chest X-rays, *Computers and Biomedical Research*, 12:1-15, 1979
- [20] Katsuragawa S., Doi K. and MacMahon H. Image Feature Analysis and Computer-Aided Diagnosis in Interstitial Lung Disease in Digital Radiography: Detection and Characterization of Interstitial Lung Disease in Digital Chest Radiographs, *Medical Physics*, 15:311-319, 1988

- [21] Katsuragawa S., Doi K. and MacMahon H. Image Feature Analysis and Computer-Aided Diagnosis in Interstitial Lung Disease in Digital Radiography: Classification of Normal and Abnormal Lungs with Interstitial Disease in Chest Images, *Medical Physics*, 16:38-44, 1989
- [22] Katsuragawa S., Doi K., MacMahon H., Nakamory N., Sasaki Y. and Fennessy J. Quantitative Computer-Aided Analysis of Lung Texture in Chest Radiographs, *RadioGraphics*, 10(2):257-269, 1990
- [23] Katsuragawa S., Doi K., MacMahon H., Monnier-Cholley L., Morishita J. and Ishida T. Quantitative Analysis of Geometric Pattern Features of Interstitial Infiltrates in Digital Chest Radiographs: Preliminary Results, *Journal of Digital Imaging* 9(3):137-144, 1996
- [24] Kheddache S., Denbratt L. and Angelhed J.E. Digital Chest Radiography - Optimizing Image Processing Parameters for the Visibility of Chest Lesions and Anatomy, *European Journal of Radiology*, 22:241-245, 1996
- [25] Kido S., Ikezoe J., Naito H., Tamura S. and Machi S. Fractal Analysis of Intersitial Lung Abnormalities in Chest Radiography, *RadioGraphics*, 15:1457-1464, 1995
- [26] Kido S., Tamura S., Nakamura H. and Kuroda C. Interstitial Lung Diseases: Evaluation of the Performance of a Computerized Analysis System versus Observers, *Computerized Medical Imaging and Graphics*, 23:103-110, 1999
- [27] Kido S. and Tamura S. Computerized Classification of Interstitial Lung Abnormalities on Chest Radiographs with Normalized Radiographic Index and Normalized Fractal Dimension, *European Journal of Radiology*, 37:184-189, 2001
- [28] Koss E.J., Newman T.K., Johnson K.T. and Kirch L.D., Abdominal Organ Segmentation Using Texture Transforms and a Hopfield Neural Network, *IEEE Transactions on Medical Imaging*, 18(7):640-648, 1999
- [29] Kruger R.P., Thompson W.B. and Turner A.F. Computer Diagnosis of Pneumoconiosis, *IEEE Transactions on Systems, Man and Cybernetics*, 4:40, 1974
- [30] Li Q., Katsuragawa S., Ishida T., Yoshida H., Tsukuda S., MacMahon H. and Doi K. Contralateral Subtraction: A Novel Technique for Detection of Asymmetric Abnormalities on Digital Chest Radiographs, *Medical Physics*, 27(1):47-55, 1999
- [31] Miro S., Leung L.A., Rubin kD.G., Choi Y.H., Kee T.S., Mindelzun E.R., Startk P., Wecler L., Plevritis K.S. and Betts J.B. Digital Storage Phosphor Chest Radiography: An ROC Study of the Effect of 2K versus 4K Matrix Size on Observer Performance, *Radiology*, 218(2):527-539, 2001
- [32] Monnier-Cholley L., MacMahon H., Katsuragawa S., Morishita J. and Doi K. Computerized Analysis of Interstitial Infiltrates on Chest Radiographs: A New Scheme Based on Geometraic Pattern Features and Fourier Analysis, *Academic Radiology*, 2:455-462, 1995
- [33] Morishita J., Doi K., Katsuragawa S., Monnier-Cholley L. and Hever M. Computer-Aided Diagnosis for Interstitial Infiltrates in Chest Radiographs: Optical-Density Dependence of Texture Measre, *Medical Physics*, 22(9):1515-1522, 1995
- [34] Nakamura K., Yoshida H., Engelmann R., MacMahon H., Katsuragawa S., Ishida T., Ashizawa K. and Doi K. Computerized Analysis of the Likelihood of Malignancy in Solitary Pulmonary Nodules with Use of Artificial Neural Networks, *Radiology* , 214(3):823-830, 2000
- [35] Park M., Wilson L. and Jin J. Automatic Extraction of Lung Boundaries by a Knowledge-Based Method, *Visual Information Processing*, 2:11-16, 2001
- [36] Park M., Jin J., and Wilson L. Fast Conect-based Image Retrieval Using quasi-Gabor Filter and Reduction of Image Feature, 5th IEEE Southwest Symposium on Image Analysis and Interpretation, 178-182, 2002a
- [37] Park M., Jin J., and Wilson L. Hierarchical Indexing Images Using Weighted Low Dimensional Texture Feature, 15th IAPR International Conference on Vision Interface, 39-44, 2002b
- [38] Park M., Jin J., and Wilson L. A New Texture Analysis Method for Classification of Interstitial Lung Abnormalities in Chest Radiography, 7th International Conference on Control, Automation, Robotics and Vision, 1636-1640, 2003
- [39] Park M., Jin J., and Wilson L. Lung Texture Analysis using 3D Classification, The image Processing of Medical Imaging Conference at SPIE, 2004, (accepted)
- [40] Reddy B.S. and Chatterji B.N. An FFT-Based Technique for Traslation, Rotation, and Scale-Invariant Image Registration, *IEEE Transactions on Image Processing*, 5(8):1266-1271, 1996
- Revesz J. and Kundel H.L. Feasibility of Classifying Disseminated Diseases Based on their Fourier Spectra *Investigative Radiology*, 8:345-349, 1973
- [41] Sridhar B., Phatak A. and Chatterji G., Scene segmentation of natural images using texture measures and back-propagation, NASA, Tech Memo. 104003:24, 1993
- [42] Stark H. and Lee D. An Optical-digital Approach to the Pattern Recognition of Coal Workers' Pneumoconiosis, *IEEE Transactions on Systems, Man and Cybernetics*, SMC-6(11):788-793, 1976
- [43] Teuner A. and Hosticka B.J. Adaptive filter for two-dimensional Gabor Transformation and Its Implementation, *IEE Proceedings-1*, 140(1):2-6, 1993
- Tully R.J., Connors R.W., Harlow C.A. and Larsen G.N. Interactive Analysis of Pulmonary Infiltration. *Proceedings of the 3rd International Joint Conference on Pattern Recognition*, 238-242, 1976
- [44] Tully R.J., Connors R.W., Harlow C.A. Toward Computer Analysis of Pulmonary Infiltration *Investigative, Radiology*, 13:298-305, 1978
- [45] Turner A.F., Kruger R.P. and Thompson W.B. Automated Computer Screening of Chest Radiographs for Pneumoconiosis, *Investigative Radiology*, 11(4):258-266, 1976
- [46] Wang L., Chen C. and Lin W. An Efficient Algorithm to Compute the Complete Set of Discrete Gabor Coefficients, *IEEE Transactions on Image Processing*, 3(1):8782, 1994
- [47] Weiser W.J. Sorting Out Intersitial Lung Disease, *Applied Radiology*, 58-65, 1993
- [48] Wilson L.S. Description of Broad-Band Pulsed Doppler Ultrasound Processing using the Two-Dimensional Fourier Transform, *Ultrasonic Imaging*, 13:301-315, 1991

Mira Park received the M.S. and PhD degree in the computer science engineering from the University of New South Wales in 2003. During 2004-2005, she worked as a research fellow in the computer science and software engineering at the University of Melbourne. She is a research fellow in the school of design, communication and IT of the Newcastle University.